Dalton Transactions

Accepted Manuscript

ROYAL SOCIETY OF CHEMISTRY

www.rsc.org/dalton

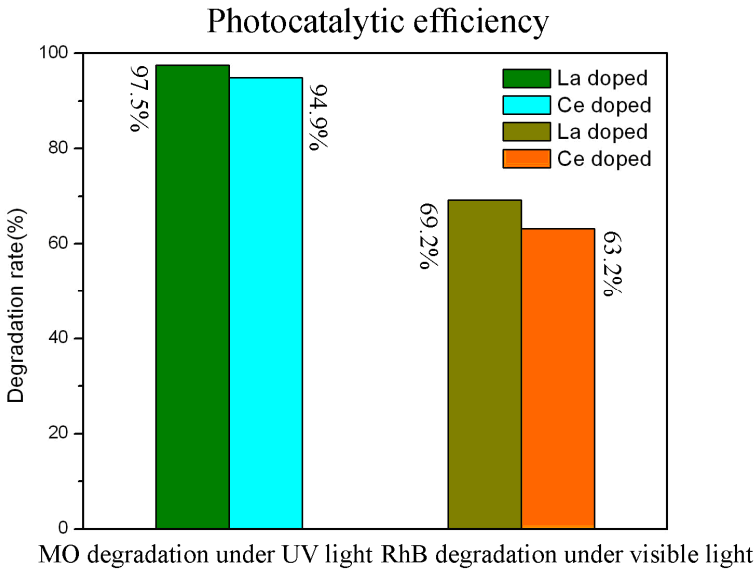

La^{3+}-$H_3PW_{12}O_{40}$ and Ce^{3+}-$H_3PW_{12}O_{40}$ photocatalysts were synthesized by the PEG-1000 assisted hydrothermal method. These prepared photocatalysts exhibited highly efficient light-driven photocatalytic activity for the degradation of dyes (MO and RhB) under UV- and visible light irradiation.

Title Page

Photocatalytic degradation of organic dyes by La^{3+}/Ce^{3+}-$H_3PW_{12}O_{40}$ under different light irradiation

Taohai Li, Quanguo Li, Jing Yan, Feng Li *

College of Chemistry, Key Lab of Environment Friendly Chemistry and Application in Ministry of Education, Xiangtan University, Xiangtan, 411105, China

* Corresponding author. Tel.: +86-731-5829-2206; fax: +86-731-5829-2251;
E-mail address:fengli_xtu@hotmail.com

Abstract

New photocatalysts (La^{3+}-$H_3PW_{12}O_{40}$ and Ce^{3+}-$H_3PW_{12}O_{40}$) were prepared, and the degradation activity of these products was evaluated. These photocatalysts were synthesized by hydrothermal method assisted by PEG-1000 from the reactions of $LaCl_3$ or $CeCl_3$ and phosphotungstic. The prepared catalysts were characterized by X-ray diffraction (XRD), Fourier transform infrared spectroscopy (FT-IR), scanning electron microscopy (SEM), ultraviolet–visible diffuse reflection spectroscopy (UV–vis) and thermal gravimetric analysis (TGA). The catalytic activity of La^{3+}-$H_3PW_{12}O_{40}$ and Ce^{3+}-$H_3PW_{12}O_{40}$ was evaluated by adopting methyl orange (MO) and Rhodamine B (RhB) as the model dyes, and the reaction was carried out under UV- and visible light irradiation.

Keywords: Hydrothermal synthesis; Photocatalyst; Polyxometalate; Organic dyes.

1. Introduction

Photocatalytic techniques have attracted much attention due to their potential applications in water treatment, air purification and sunlight utilization. Semiconductors are efficient photocatalysts for the degradation of organic dyes, such as TiO_2 and ZnO[1-3]. In recent years, polyxometalates(POMs) have attracted particular interest in photocatalysis due to their strong Brönsted acidity and their structural properties[4, 10]. It is well known that the heteropolyacids could play the role of efficient photoinduced electron traps, enhancing the photocatalytic process and diminishing the electron hole recombination[11, 12]. However, most of the studies on photooxidative behavior of heteropolyacids were carried out with homogeneous solutions. The major disadvantage in the practical applications of these systems is the high water solubility of heteropolyacids, which makes the recovery and the reuse of the photocatalysts difficult [13, 14]. In order to overcome this disadvantage, there are two conventional methods: (1) immobilize the POMs on high-surface-area solid supports, such as zeolite, SiO_2 or TiO_2; (2) precipitate them with large monovalent cations such as K^+, Cs^+, or NH_4^+ to form insoluble salts[15-17]. In addition, we found that doping rare earth ions can also change the solubility of POMs. The rare earth ions have the ability to form complexes with various Lewis bases in the interaction of these functional groups with the f-orbital[18]. Accordingly, the incorporation of rare earth ions into heteropolyacids crystalline matrices will provide a potential method to inhibit the combination of photohole and photoelectron pairs, which will enlarge the light adsorption, and enhance the visible light photocatalytic activity.

It is well known that the UV light only accounts for small percentage (about 5%) of the sunlight, and the photodegradation of organic dyes by heteropolyacids is mainly driven by UV light, which limits the application of heteropolyacids as a photocatalyst[19, 20]. Therefore, it is necessary to synthesize efficient photocatalysts in utilizing sunlight. In the past years, there have been many reports about the applications of phosphotungstic acid in acidic or redox catalytic reactions, which supported by various materials: active carbon, silica, titania, resin, aluminas,

MCM-41, polymers, etc[21-31]. However, the preparation of rare-earth-doped phosphotungstic acid materials and their photocatalytic property have been reported rarely so far. In this paper, we adopted the simple hydrothermal method to synthesize La^{3+}/Ce^{3+}-loaded $H_3PW_{12}O_{40}$ photocatalysts. The photocatalytic activities of La^{3+}/Ce^{3+}-$H_3PW_{12}O_{40}$ were evaluated by the photodegradation of MO and RhB under UV and visible light irradiation. All products showed excellent photocatalytic activity.

2. Experimental

2.1 Chemicals

Phosphotungstic acid ($H_3PW_{12}O_{40}$) was purchased from Tianjin Chemical Reagent Factory (Tianjin China), and $LaCl_3 \cdot nH_2O$ was purchased from shanghai shanpu chemical engineering Co. Ltd (Shanghai China). $CeCl_3 \cdot 7H_2O$ was purchased from Sinopharm Chemical Reagent Co. Ltd (Shanghai China). Methyl orange (MO) and Rhodamine B (RhB) were purchased from Sinopharm Chemical Reagent Co. Ltd (Shanghai China). All the chemical reagents were of analytical grade and used as received without further purification. All the solutions were prepared using deionized water.

2.2. Preparation of La^{3+}/Ce^{3+}-$H_3PW_{12}O_{40}$ samples

In a typical synthesis of La^{3+}/Ce^{3+}-$H_3PW_{12}O_{40}$ powders, phosphotungstic acid (0.5 g) was dissolved in distilled water (15 mL), and stirred for 10 min until a clear solution was formed. Then, $LaCl_3 \cdot nH_2O$/$CeCl_3 \cdot 7H_2O$ (0.25 g) and PEG-1000 (0.2 g) were added into the solution with vigorous stirring. The obtained white aqueous solution was then transferred into a Teflon-lined autoclave, and maintained at 120 °C for 12 or 24 h. The white solid precipitate obtained later was centrifugally separated from a supernatant, which was washed with distilled water and absolute ethanol, and dried in a drying oven at 60 °C for 12 h. The La^{3+}/Ce^{3+}-$H_3PW_{12}O_{40}$ products prepared at different reaction time were denoted here as LaPW-12, LaPW-24, CePW-12, and CePW-24, respectively.

2.3. Characterization

The samples were characterized by X-ray powder diffraction (XRD) using a

MiniFlex Ⅱ X-ray diffractometer operated at 40 kV and 40 mA using Cu Kα1 radiation (λ =0.15406 nm). The scanning electron microscopy (SEM) images were obtained on JEOL JSM-6360. UV vis DRS was performed on a Hitachi U-3010, and $BaSO_4$ was used as a reference. Fourier transform infrared spectra (FT-IR) were recorded on a Perkin-Elmer 1600 FT-IR spectrometer with a KBr disk. The thermal stability of the product was monitored by using thermal gravimetric analysis (TG, TA instrument, Q50) at a heating rate of 20 ^{o}C min^{-1} from room temperature to 600 ^{o}C UV-vis absorption spectra and diffuse reflectance spectra (DRS) were recorded on a Lambda25 UV/vis spectrophotometer (Perkin-Elmer, USA). The content of La and Ce in products was detected by Inductive Coupled Plasma Emission Spectrometer (ICP) from Yanzhou Tianhe Chemical Technology Co., Ltd. The mass ratios were 1.89% (LaPW-12), 1.92% (LaPW-24), 1.13% (CePW-12) and 1.96% (CePW-24), respectively.

2.4. Evaluation of photocatalytic activity

The photochemical reactor consists of optical quartz glass beaker surrounded by a water jacket to keep the reaction at room temperature. The photocatalytic activities of La^{3+}/Ce^{3+}-$H_3PW_{12}O_{40}$ catalysts were evaluated by the degradation of MO and RhB under a 300 W UV lamp and a 300 W Xe lamp (with the 400 nm cutoff filter) irradiation, respectively (Beijing tianmai henghui light source Co. Ltd). Typically, 25 mg of solid and 50 mL of dye aqueous solution were mixed with stirring. The adsorption-desorption equilibrium of the dye on the catalyst surface was reached by keeping the solution in dark for 30 min. During irradiation, 3 mL of the suspension was extracted at certain intervals. The MO/RhB concentration was determined by its maximum absorption band.

3. Results and discussion

3.1. Structure and morphology of the samples

The phase compositions and crystal structures of the resulting powders were investigated by XRD. The X-ray diffraction patterns of the samples (LaPW-12 and LaPW-24) were shown in Fig. 1a. All of the diffraction peaks of the samples could be

well indexed to the pure phase (JCPDS PDF# 50-0657). No peaks assignable to impurity phases were detected. The cell parameters were determined to be a = 12.13 Å, b = 12.13 Å, c = 12.13 Å. Characteristic lines of pure $H_3PW_{12}O_{40}$ are at 2θ = 10.3°, 25.3° and 34.6°[32-34]. The sharp diffraction peaks indicate that the photocatalysts LaPW-12 have a good crystallinity. However, the XRD patterns at 10.3° shifted to a smaller degree slightly, and the patterns at 25.3° and 34.6° have broad diffraction peaks. These diffraction peaks can not be assigned to pure $H_3PW_{12}O_{40}$ totally, which may be attributed to the La^{3+} doped to the Keggin structure. The crystallinity of the sample heated for 12 h during the preparation process was very similar to that heated for 24 h. Fig. 1b shows the XRD patterns of the samples CePW-12 and CePW-24 obtained in different conditions. The diffraction peaks of the Ce^{3+} -$H_3PW_{12}O_{40}$ corresponded to the standard phase-pure $H_3PW_{12}O_{40}$ (JCPDS PDF# 50-0657), and no peaks of impurities were detected from this pattern. Compared with LaPW-12 and LaPW-24, doping with Ce^{3+} did not change the diffraction angles, which may be due to the low doping amount of Ce^{3+} in the catalysts. It suggested that doping with rare earth ions did not change the crystal structure of $H_3PW_{12}O_{40}$ significantly. As shown in Fig. 1a and b, the strong and sharp peaks indicated high crystallinity of the as-prepared samples. Moreover, the sharp diffraction peaks indicated that the photocatalysts (LaPW-12 and CePW-12) have a better crystallinity than other two samples, which demonstrated the reaction time have an effect on the crystallinity.

Fig. 1.

The morphology and microstructure of the samples synthesized by the hydrothermal method in different synthesis conditions were observed by SEM. Fig. 2a showed the SEM micrographs of LaPW-12 heated at 120 □ for 12 h during the preparation process. As shown in Fig. 2a, relative uniform microrods formed with length of 100–500 nm and width of 20–90 nm. Fig. 2b showed the SEM micrographs of LaPW-24, and the morphology of LaPW-24 was different from that of LaPW-12. Large flakes in micrometer size were observed in LaPW-24, which showed the significant influence of reaction time on their morphology. In addition, some spherical

particles were observed in both LaPW-12 and LaPW-24. Fig. 2c and 2d showed the SEM micrographs of CePW-12 and CePW-24. The similar morphology of flaky crystals of CePW-12 and CePW-24 indicated that reaction time did not change the morphology of samples. The morphology of samples revealed that all four samples were composed of many smaller building blocks, which were quite common in a self-assembly process.

Fig. 2.

To confirm the crystal structure, Fourier transform infrared (FT-IR) spectroscopy was performed on the as-prepared samples. Fig. 3a presented the FT-IR spectra of LaPW-12 and LaPW-24. As shown in Fig. 3a, the characteristic bands of the Keggin anion kept at the range of 700-1100 cm^{-1} in samples with La^{3+} doping, which showed that the keggin structure remains during the doping process. In the IR spectrum, the main absorption bands of H_3PW_{12} Keggin anion at 400–1000 cm^{-1} were attributed to P-Oa (1079 cm^{-1}), W=Ot (979 cm^{-1}), W-Oc-W (895 cm^{-1}) and W-Oe-W (801.5 cm^{-1}), where a, t, c and e stand for the specific positions (internal, terminal, corner and edge-shared, respectively) of different oxygen atoms in Keggin structure [5, 35]. The FT-IR spectra of CePW-12 and CePW-24 with different reaction time were shown in Fig. 3b. It showed the same keggin structure as Fig. 3a. The presence of organic groups is confirmed by the band of $-CH_2$ around 2800–3000 cm^{-1}. The observed bands at 1635, 1560 cm^{-1} and broad stretching bands in the 3000–3500 cm^{-1} were ascribed to physical absorbed water on the sample surface [36, 37]. It can be concluded that the keggin structure was not destroyed by doping of La^{3+}/Ce^{3+}. However, the stretching vibration of LaPW-12 and CePW-12 were stronger than those of LaPW-24 and CePW-24. This implied that different reaction time had effect on products.

Fig. 3.

Generally, photocatalytic activity is governed by various factors such as optical absorption property,, phase structure, surface area, interfacial charge transfer, and the separation efficiency of photo-induced electron–hole pairs[38]. To investigate the optical absorption properties of samples, the UV-visible absorption spectra of these

substances were measured (Fig. 4a). LaPW-12 and LaPW-24 exhibited a strong absorption in the region of UV-visible light, and LaPW-24 showed the enhanced visible-light absorption. Therefore, the reaction time affected the optical absorption properties. LaPW-12 had a greater optical absorption capability than LaPW-24. As shown from Fig. 4b, the UV-visible absorption spectra of CePW-12 and CePW-24 are similar with LaPW-12 and LaPW-24. The absorption value of CePW-12 is lower than CePW-24. The characteristic band at 255 nm corresponded to the oxygen-tungsten charge transfer transition [39].

Fig. 4.

The TGA curves of LaPW-12 and CePW-12 were shown in Fig. 5. As shown in Fig. 5(a), there are two obvious mass losses curves for LaPW-12. The first one started at 57 ^{o}C and ended at 191 ^{o}C with a weight loss of 1.5%, which can be attributed to the evaporation of water adsorbed in samples. The second loss was observed at 370 ^{o}C with a weight loss of 8.5%. For CePW-12, there is a continuous decrease from 60 ^{o}C to 320 ^{o}C with a weight loss of 6.4 %, which may be due to more crystal water adsorbed in the sample. There was a lost at 370 ^{o}C for either LaPW-12 or CePW-12, which corresponded to the decomposition of $H_3PW_{12}O_{40}$, the vaporization and elimination of volatile products [40].

Fig. 5.

3.2. Photocatalytic activity under UV light irradiation

The photocatalytic activities of the as-prepared samples were evaluated by the degradation of the typical organic contaminant MO/RhB under light irradiation. Before the photocatalytic reaction was carried out, the MO/RhB solution (10 mg/L) was first photolyzed in the absence of the photocatalyst. The result showed that MO/RhB was not decomposed with enough irradiation, and after the photocatalyst reaching the adsorption–desorption equilibrium, the concentration of MO did not change in dark with the increasing of the retention time. Therefore, both photocatalyst and illumination are the necessary conditions for efficient degradation.

Fig. 6a and 6c showed the changes in the intensity of maximal absorption peak of

MO at 464 nm for the LaPW-12 and LaPW-24 under UV irradiation. The absorption peak at 464 nm decreased gradually with increasing of the retention time, and disappeared after 25 min. No new absorption bands appeared in the spectrum, which indicated the total decomposition of MO aqueous solution during the reaction [41]. The detailed photocatalytic efficiency of the as-prepared samples was shown in Fig. 6 (b) and (d). With UV-light irradiation for 25 min, the LaPW-12 exhibit enhanced photocatalytic activity. The degradation rates of MO are about 97.5% and 68.8% for LaPW-12 and LaPW-24 samples, respectively. However, the degradation efficiency of MO increased obviously with the addition of photocatalyst. It can be inferred that UV-light and photocatalyst promoted the photocatalytic reaction together.

Fig. 6.

Fig. 7 (a) and (c) showed the temporal evolution of the spectral changes in the intensity of the maximal absorption peak of the MO at 464 nm under UV irradiation. As shown in Fig. 7, the absorption peak at 464 nm decreased gradually with the increasing of the retention time, and tended to disappear after 25 min. The photocatalytic property of samples heated for 12 h during the preparation process was superior to that heated for 24 h. No new absorption bands appeared in the spectrum, which indicated the complete decomposition of the MO aqueous solution during the reaction. The detailed photocatalytic rate of the as-prepared samples was shown in Fig. 7 (b) and (d). With the irradiation of 25 min, the CaPW-12 exhibited better photocatalytic activity than CePW-24. The degradation rates of MO are about 94.8% and 89.1% for CePW-12 and CePW-24, respectively.

Fig. 7.

3.3. Photocatalytic activity under visible light irradiation

The photocatalytic activity of the samples was also evaluated by the photodegradation of RhB. Fig. 8a and c showed the UV-vis absorption spectrum of the aqueous solution of RhB (initial concentration: 5 mg/L, 30 ml) with 25 mg of LaPW-12 and LaPW-24 exposed to the visible light for various durations, respectively.

As shown in Fig. 8, the characteristic absorption of RhB at 550 nm decreased rapidly with the increasing of the exposure time, and the degradation rate reached 80% after 150 min. Thus, the photocatalytic property of samples heated for 12 h during the preparation process was superior to that heated for 24 h. As a comparison, Fig. 8b and 8d showed the degradation of RhB exposed to xenon light, where photocatalyst heated for 12 h and 24 h during the preparation process were also investigated, respectively. Without any photocatalyst, only a slow decreasing for the concentration of RhB was detected under visible light irradiation, which was similar to the situation of existence of photocatalyst without visible light irradiation. However, the degradation rate of RhB increased with the addition of photocatalyst obviously. It can be concluded that the catalysis of photocatalytic reaction was attributed to the synergistic effect of visible light and photocatalyst.

Fig. 8.

As shown in Fig. 9, the photocatalytic performance of Ce^{3+}-$H_3PW_{12}O_{40}$ was evaluated by the photocatalytic degradation of RhB under visible light irradiation. Fig. 9a and 9c showed the decrease in UV-vis absorption intensity of the solution of RhB with time (recorded at 30 min intervals). We observed that the photodegradation rate was over 50% after 90 min under visible light irradiation. As shown in Fig. 9, the characteristic absorption of RhB at 550 nm diminished rapidly with the increasing of the exposure time. It showed that the photocatalytic property of samples CePW-24 was superior to CePW-12. As a comparison, we observed that RhB was very stable under visible light irradiation without any catalyst. However, the degradation efficiencies of RhB without light was better than that of La^{3+}-$H_3PW_{12}O_{40}$, which was due to the stronger adsorption capacity of Ce^{3+}-$H_3PW_{12}O_{40}$ with special morphology which accelerated the degradation of RhB solution.

Fig. 9.

Herein, we compared the degradation efficiency of La^{3+} and Ce^{3+} doped phosphotungstic acid with the reported dyes and light sources, respectively. Fig.10a shows the degradation rate of methyl orange under UV light irradiation for 15min. As

shown in Fig. 10a, both LaPW-12 and CePW-12 showed excellent photocatalytic activity. The degradation rate of LaPW-12 for MO was 97.5%, which was greater than that of CePW-12 (94.9%). Fig.10b showed the degradation rate of LaPW-12 and CePW-12 for RhB under visible light irradiation for 90 min. The degradation rate of LaPW-12 and CePW-12 for RhB was 69.2% and 63.2%, respectively, which showed that the photocatalytic activity of La^{3+}-$H_3PW_{12}O_{40}$ was better than that of Ce^{3+}-$H_3PW_{12}O_{40}$. This may be because the radius of Ce^{3+} is smaller than that of La^{3+}. The smaller radius means stronger electron affinity, so the affinity electron of Ce^{3+} is better than that of La^{3+}. When the ability of capturing electron is strong enough, they become the hole-electron recombination centers, so the lower effective electrons and holes resulted in the decrease of catalytic activity. Fig.10 also illustrated the electronic excitation efficiency of UV light was much better than that of visible light. Therefore, we will study the visible light response of new photocatalyst with high efficiency further.

Fig. 10.

Since it can reduce the cost of the process significantly, the reuse of products in photocatalytic processes has attracted considerable attention, which is very important in the applicability of photocatalysis. In order to evaluate the efficiency of reused photocatalysts, a series of experiments were performed at the catalyst loading of 2g/L. As shown in Fig. 11, photocatalytic efficiency still remained sufficiently high in the three reusing cycles. In the fourth reuse cycle, the photocatalytic efficiency(degradation of RhB) of CePW-12 decreased faster than others. Minor losses in the amount of CePW-12 have a relatively large impact, which could explain the decreasing photocatalytic rate after reuse. The above results suggest that the La^{3+}/Ce^{3+}-$H_3PW_{12}O_{40}$ photocatalysts are stable and can be reused.

Fig. 11.

Fig.12 showed the XRD patterns of LaPW-12 and CePW-12 before and after 150 min of UV light irradiation. Both the position and the intensity of the peaks in the XRD pattern were almost same with those of sample before irradiation. As shown in the results, samples were considered to be very stable under the present experimental

conditions.

Fig. 12.

To study the effect of the structure of the catalysts on photodegradation, the mechanism of photocatalytic reaction was studied. Photogenerated electron-hole pairs formed when photocatalyst was irradiated by UV/visible light. The inspired electrons will overcome their mutual electrostatic attraction, separate and transfer to the surface, where the electrons will be captured by O_2, and the holes will be transferred by adsorbed hydrogen to form O^{2-} and ·OH radicals (as shown in (1)-(7)).

$$H_2O \rightarrow H^+ + OH^- \quad (1)$$

$$h^+ + OH^- \rightarrow OH^- \quad (2)$$

$$e^- + O_2 \rightarrow O_2^- \quad (3)$$

$$\cdot O_2^- + H^+ \rightarrow HO_2\cdot \quad (4)$$

$$2HO_2\cdot \rightarrow H_2O_2 + O_2 \quad (5)$$

$$H_2O_2 + O_2^- \rightarrow OH + OH^- + O_2 \quad (6)$$

$$H_2O_2 + h\upsilon \rightarrow 2\cdot OH \quad (7)$$

The heteropolyacids ions generated from electron reduction reaction by e-CB can also synergistically catalyze the substrate molecules. Simultaneously, empty d-orbits of heteropolyacids inhibit the recombination of the electrons and holes. Rare earth ions doping lead to a new electronic state in the middle of the heteropolyacids band gap. The introduction of structural defects into the heteropolyacids crystal lattice leads to the change of band gap energy [42]. The schematic diagram of the photocatalytic mechanism was shown in Fig. 13.

Fig. 13.

4. Conclusions

In summary, La^{3+}/Ce^{3+}-$H_3PW_{12}O_{40}$ photocatalysts were synthesized by facile hydrothermal process successfully. These photocatalysts exhibited highly efficient

light-driven photocatalytic activity for degradation of dyes (MO and RhB). It is due to the synergistic effect existed between the rare earth ions and heteropolyacids, which can enlarge the light adsorption and inhibit the recombination of photogeneration electron-hole pairs. It confirmed that doping rare earth ions is a desirable way to avoid the high recombination rate of electrons-holes of photocatalysts. Therefore, the photocatalytic activity of the La^{3+}-loaded samples was higher than that of Ce^{3+}-loaded samples. We believe that our strategy of synthesizing La^{3+}/Ce^{3+}-$H_3PW_{12}O_{40}$ for enhancing photocatalytic activity will have a considerable impact on the development of highly efficient visible-light photocatalysts for the degradation of organic pollutants.

Acknowledgment

The authors acknowledge with thanks the financial support of Provincial Natural Science Foundation of Hunan, China (13JJ6041) and the National Natural Science Foundation of China (21343008)

References

[1] S. Sakthivel, B. Neppolian, M.V. Shankar, Sol. Energy Mater. Sol. Cells. 77 (2003) 65.

[2] M. Stylidi, D.I. Kondarides, X.E. Verykios, Appl. Catal., B: Environ. 47 (2004) 189.

[3] S. Chakrabarti, B.K. Dutta, J. Hazard. Mater. 112 (2004) 269.

[4] I.V. Kozhevnikov, Chem. Rev. 98 (1998) 171.

[5] T. Okuhara, N. Mizuno, M. Misono, Adv. Catal. 41 (1996) 113.

[6] M. Li, C. Xu, J.S. Ren, Chem. Commun. 49 (2013) 11394.

[7] W.H. Zhou, M.H. Cao, N. Li, S.Y. Su, Mater Res. Bull. 48 (2013) 2308

[8] T. Kida, H. Matsufuji, M. Yuasa, Adv. Mater. Res. 747 (2013) 518.

[9] J. Zhang, W.L. Chen, E.B. Wang, Inorg. Chem. Commun. 38 (2013) 96.

[10] A. Seliverstov, C. Streb, Chem. Commun. 50 (2014) 1827.

[11] P. Ngaotrakanwiwat, S. Saitoh, Y. Ohko, Phys. Chem. Chem. Phys. 5 (2003) 3234.

[12] D.A. Friesen, L. Morello, J. Photochem. Photobiol. A: Chem. 133 (2000) 213.

[13] M.J. Piao, K. Xu, J.L. Adv. Mater. Res. 610 (2013) 68.

[14] R.R. Ozer, J.L. Ferry, J. Phys. Chem. B. 106 (2002) 4336.

[15] C.C. Chen, Q. Wang, Environ. Sci. Technol. 40 (2006) 3965.

[16] J. Haber, K. Pamin, App. Catal. A: General. 256 (2003) 141.

[17] P. Dupont, F. Lefebvre, J. Mole. Catal. A: Chemical. 114 (1996) 299.

[18] H.X. Shi, T.Y. Zhang, J. Coll. Inter. Sci. 380 (2012) 121.

[19] Y.H. Guo, C.W. Hu, J. Mol. Catal. A: Chem. 262 (2007) 136.

[20] C.C. Chen, X.Z. Li, J. Phys. Chem. B. 106 (2002) 318.

[21] M.A. Schwegler, P. Vinke, Appl. Catal. A: General. 80 (1992) 41.

[22] I.V. Kozhevnikov, A. Sinnema, Catal. Lett. 27 (1994) 187.

[23] P. Dupont, J.C. Védrine, Appl. Catal. A: General. 129 (1995) 217.

[24] W. Chu, X. Yang, Langmuir. 12 (1996) 4185.

[25] Y. Izumi, R.Hasebe, J. Catal. 84 (1983) 402.

[26] C. Rocchiccioli-Deltcheff, M. Amirouche, J. Catal. 126 (1990) 591.

[27] S. Kasztelan, E. Payen, J.B. Moffat, J. Catal. 125 (1990) 45.

[28] V.M. Mastikhin, S.M. Kulikov, A.V. Nosov, J. Mol. Catal. 60 (1990) 65.

[29] W.C. Cheng, N.P. Luthra, J. Catal. 109 (1988) 163.

[30] K.M. Rao, R. Gobetto, J. Catal. 119 (1989) 512.

[31] T. Baba, Y. Ono, Appl. Catal. 22 (1986) 32.

[32] S.H. Chai, H.P.Wang, Appl. Catal. A: Gen. 353 (2008) 213.

[33] J.A. Dias, S.C.L. Dias, J. Chem. Soc., Dalton Trans. 3 (2001) 228.

[34] J.A. Dias, J.P. Osegovic, R.S. Drago, J. Catal. 183 (1999) 83.

[35 M.T. Pope, Heteropoly and isopoly oxometalates, Springer-Verlag, Berlin, 1983.

[36] A.L. Linsebigler, G. Lu, Chem. Rev. 95 (1995) 735.

[37] X.L. Yan, L. Zhang, Y. Zhang, Ind. Eng. Chem. Res. 50 (2011) 3220.

[38] J.G. Yu, Y. Le, B. Cheng, Rsc Adv. 2 (2012) 6784.

[39] Y.L. You, S.Y. Gao, Z. Yang, J. Colloid Interface Sci. 365 (2012) 198.

[40] S.R. Mane, R.R. Kharade, Dig J Nanomater Bios. 6 (2011) 451.

[41] X.P. Lin, T. Huang, F.Q. Huang, J. Phys. Chem. B. 110 (2006) 24629.

[42] Y.B. Xie, C.W. Yuan, Appl Catal B-Environ. 46 (2003) 251.

Figure captions

Fig. 1 XRD patterns of LaPW-12, LaPW-24(a) and CePW-12, CePW-24(b)

Fig. 2 SEM images of LaPW-12(a), LaPW-24(b) and CePW-12(c), CePW-24(d)

Fig. 3 FT-IR spectra of LaPW-12, LaPW-24(a) and CePW-12, CePW-24(b).

Fig. 4 (a)UV-vis spectra of La^{3+} doped phosphotungustic acid; (b)UV-vis spectra of Ce^{3+} doped phosphotungustic acid.

Fig. 5 (a)TG curves for (a) La^{3+} doped Phosphotungustic acid; (b) Ce^{3+} doped Phosphotungustic acid.

Fig. 6 (a) and (c) the temporal evolution of the spectra during the photodegradation of MO mediated by LaPW-12 and LaPW-24; (b) and (d) photocatalytic properties of LaPW-12 and LaPW-24 for degrading MO solution under UV light irradiation.

Fig. 7 (a) and (c) the temporal evolution of the spectra during the photodegradation of MO mediated by CePW-12 and CePW-24; (b) and (d) photocatalytic properties of CePW-12 and CePW-24 for degrading MO solution under UV light irradiation.

Fig. 8 (a) and (c) the temporal evolution of the spectra during the photodegradation of RhB mediated by LaPW-12 and LaPW-24; (b) and (d) photocatalytic properties of LaPW-12 and LaPW-24 for degrading RhB solution under visible light irradiation.

Fig. 9 (a) and (c) the temporal evolution of the spectra during the photodegradation of RhB mediated by CePW-12 and CePW-24; (b) and (d) photocatalytic properties of CePW-12 and CePW-24 for degrading RhB solution under visible light irradiation.

Fig. 10 (a) The rate of MO degradation using La^{3+}/Ce^{3+}-$H_3PW_{12}O_{40}$ under UV light irradiation , (b)The rate of RhB degradation using La^{3+}/Ce^{3+}-$H_3PW_{12}O_{40}$ under visible light irradiation.

Fig. 11 Effect of products reuse on degradation of MO and RhB after 60 min under UV light.

Fig. 12 (a) LaPW-12, (b) CePW-12, XRD patterns before and after 150 min UV light irradiation.

Fig. 13 Photocatalytic mechanism schematic diagram of La^{3+}/Ce^{3+}-$H_3PW_{12}O_{40}$.

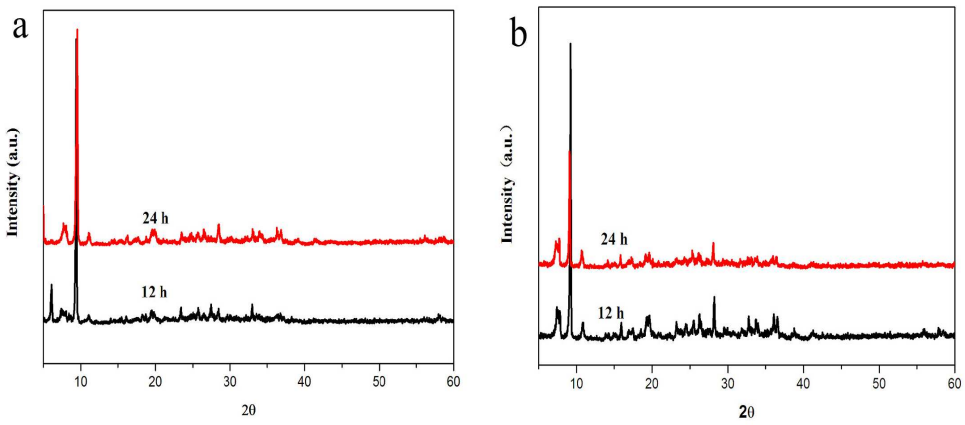

Fig. 1.

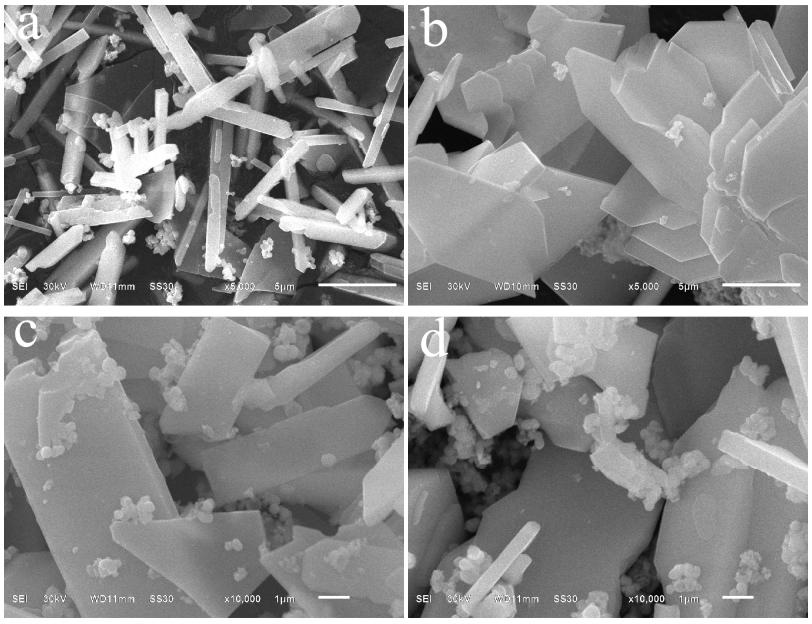

Fig. 2.

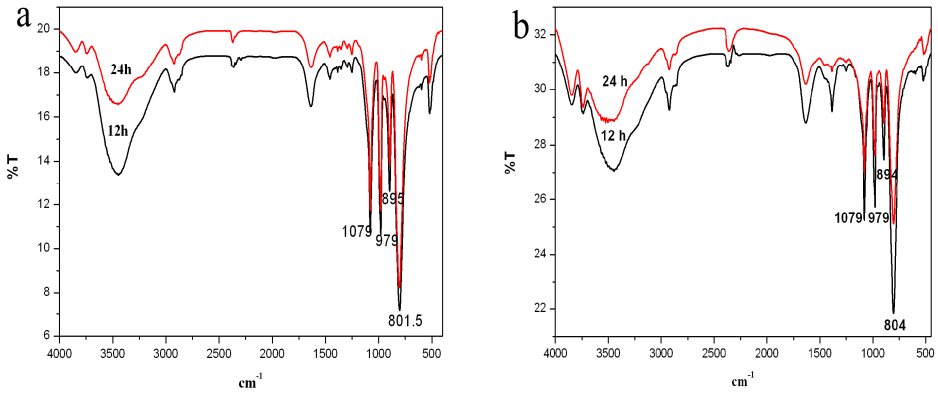

Fig. 3.

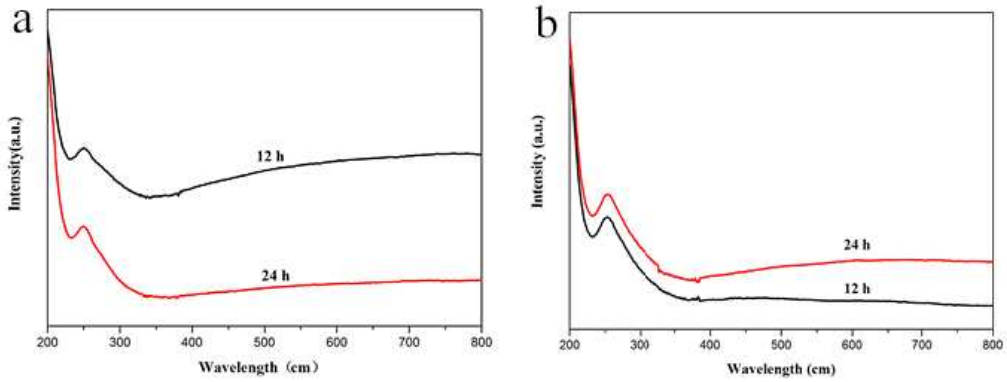

Fig. 4.

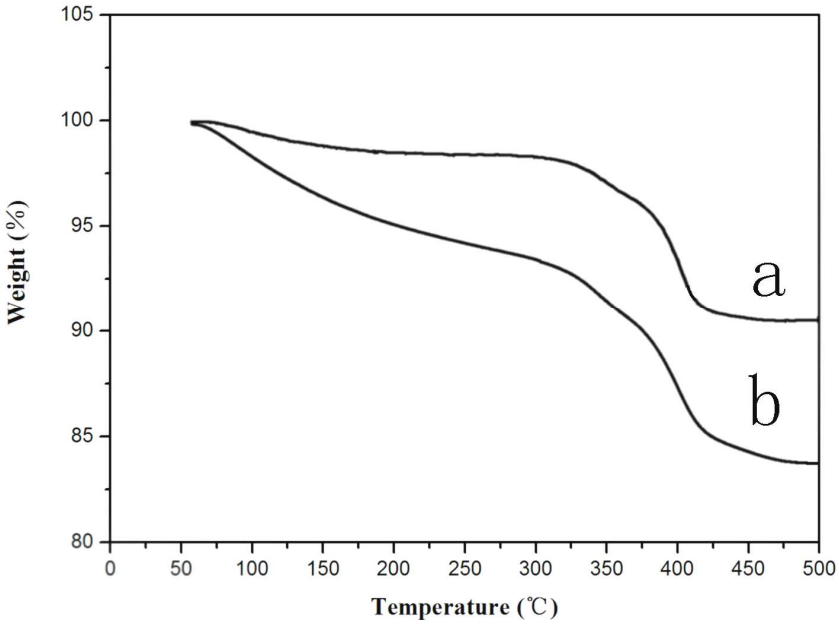

Fig. 5.

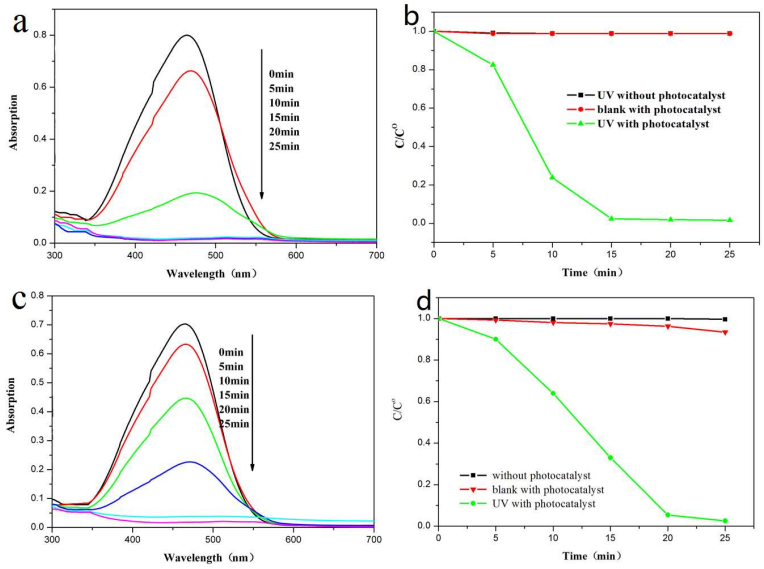

Fig. 6

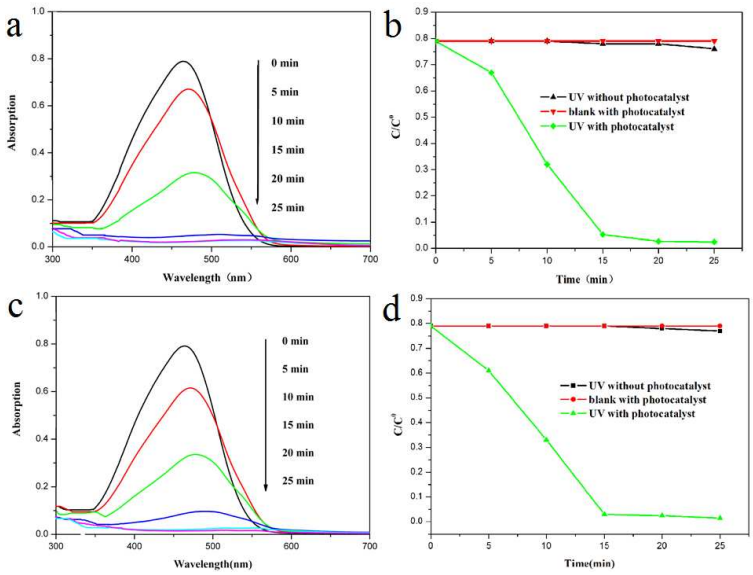

Fig. 7

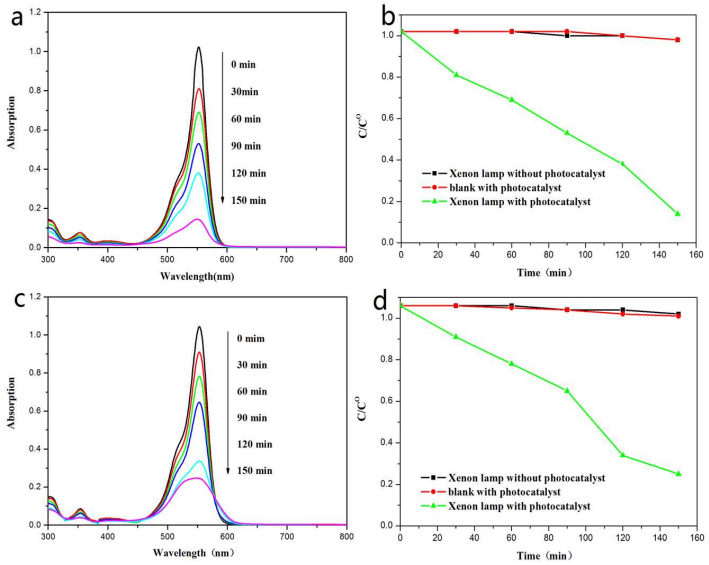

Fig. 8

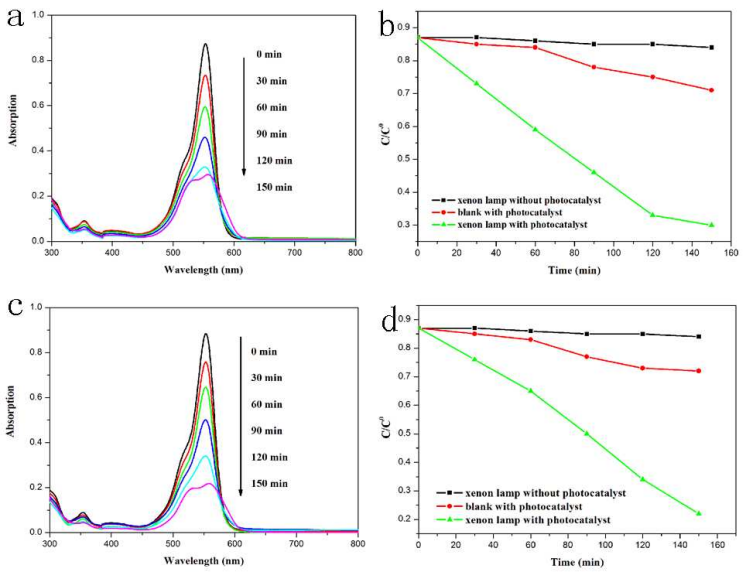

Fig. 9.

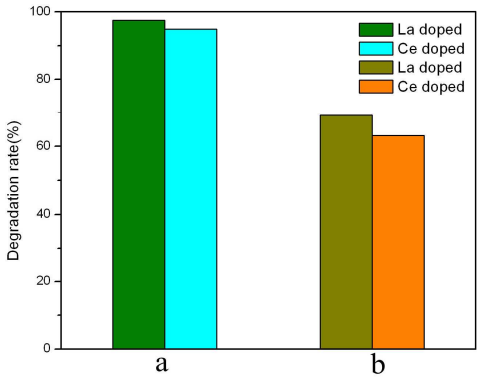

Fig. 10.

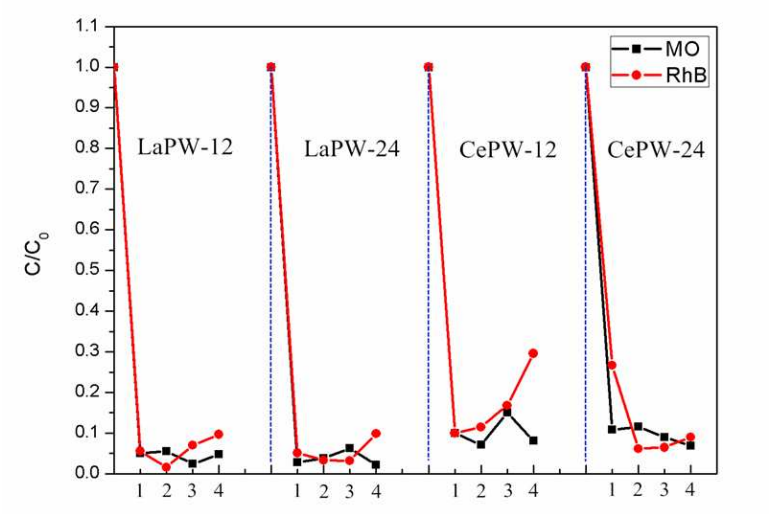

Fig. 11.

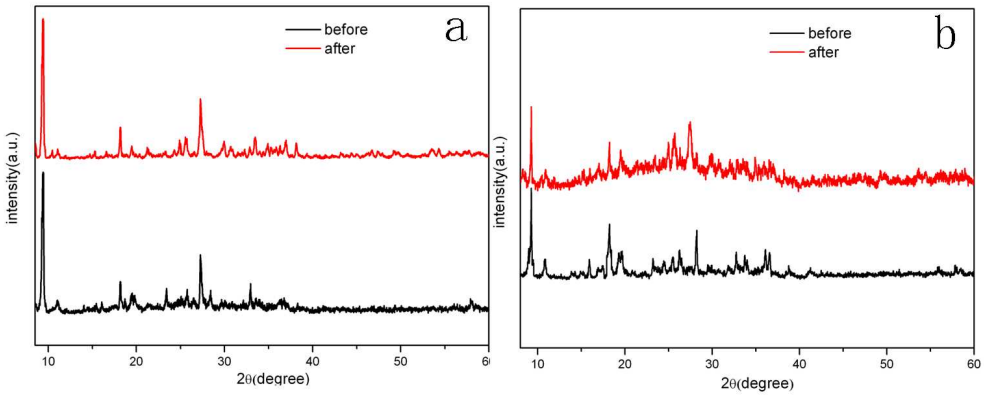

Fig. 12.

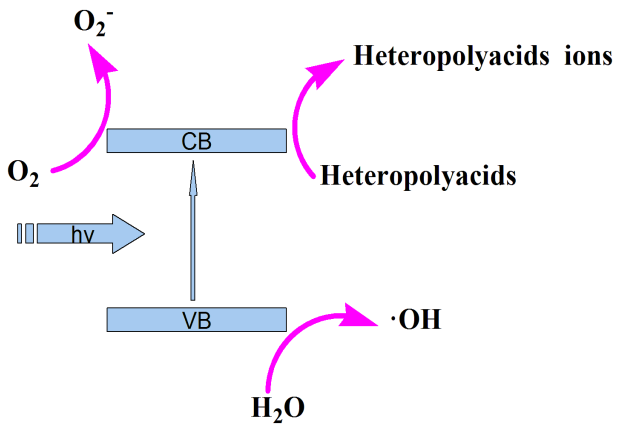

Fig. 13.